

Numerical investigation of photon creation in a three-dimensional resonantly vibrating cavity: TE-modes

Marcus Ruser*

*Département de Physique Théorique, Université de Genève,
24 quai E. Ansermet, CH-1211 Genève 4 Switzerland*

The creation of TE-mode photons in a three-dimensional perfectly conducting cavity with one resonantly vibrating wall is studied numerically. We show that the creation of TE-mode photons in a rectangular cavity is related to the production of massive scalar particles on a time-dependent interval. The equations of motion are solved numerically which allows to take into account the intermode coupling. We compare the numerical results with analytical predictions and discuss the effects of the intermode coupling in detail. The numerical simulations reveal that photon creation in a three-dimensional resonantly vibrating cavity can be maximized by arranging the size of the cavity such that certain conditions are realized. In particular, the creation of TE-mode photons in the lowest frequency mode (1, 1, 1) is most efficient in a non-cubic cavity where the size of the non-dynamical dimensions is roughly 11 times larger than the size of the dynamical dimension. We discuss this effect and its relation to the intermode coupling in detail.

PACS numbers: 03.65.-w, 03.70.+k, 12.20.Ds, 42.50.Lc

I. INTRODUCTION

In 1948 Casimir [1] predicted an attractive force between two perfectly conducting plates (ideal mirrors). This so-called Casimir effect [2, 3, 4, 5] caused by the change of the zero point energy of the quantized electromagnetic field in the presence of boundaries has been verified experimentally with high accuracy [6, 7, 8, 9, 10]. The existence of the Casimir force [11] acting on macroscopic boundaries confirms the reality of quantum vacuum fluctuations and their potential influence even on macroscopic scales.

Besides the change of the zero point energy of the quantum vacuum provoked by static boundary conditions a second and even more fascinating feature of the quantum vacuum appears when considering dynamical, i.e time-dependent boundary conditions. The quantum vacuum responds to time-varying boundaries with the creation of real particles (photons) out of virtual quantum vacuum fluctuations. This effect, usually referred to as dynamical or non-stationary Casimir effect [12], has gained growing interest during recent years.

A scenario of particular interest are so-called vibrating cavities [13] where the distance between two parallel mirrors changes periodically in time. The possibility of resonance effects between the mechanical motion of the mirror and the quantum vacuum leading to an even exponential growth of the particle occupation numbers for the resonance modes makes this configuration the most promising candidate for an experimental verification of the dynamical Casimir effect.

For a one-dimensional vibrating cavity this effect has been studied in numerous works [14, 15, 16, 17, 18, 19, 20, 21, 22, 23, 24, 25, 26, 27, 28, 29, 30, 31] showing

that the total energy inside a resonantly vibrating cavity increases exponentially in time.

The more realistic case of a three-dimensional cavity is studied in [32, 33, 34, 35, 36, 37, 38, 39]. The important difference between one- and higher-dimensional cavities is that the frequency spectrum in only one spatial dimension is equidistant while it is in general non-equidistant for more spatial dimensions. An equidistant spectrum yields strong intermode coupling whereas in case of a non-equidistant spectrum only a few or even no modes may be coupled allowing for exponential photon creation in a resonantly vibrating three-dimensional cavity [15, 33, 37]. Without intermode coupling the equations of motion for the field modes reduce to harmonic oscillators with time-dependent frequency. Particle creation can then be investigated by using an approach based on Schrödinger scattering theory [40]. Even though for higher-dimensional cavities the problem can be reduced to a single harmonic oscillator in some special cases [15] the intermode coupling cannot be neglected in general [33, 36]. (See also the discussion of the work [40] in section IX of [15].)

Field quantization inside cavities with non-perfect boundary conditions has been studied in, e.g., [41, 42] and corrections due to finite temperature effects are treated in [43, 44, 45]. The interaction between the quantum vacuum and the (classical) dynamics of the cavity has been investigated in [22, 46, 47, 48] and an approach to the dynamical Casimir effect based on stationary walls but time-dependent conductivity properties is discussed in [49].

The electromagnetic field inside a dynamical cavity can be decomposed into components corresponding to the electric field parallel or perpendicular to the moving mirror. It is then possible to introduce vector potentials for each polarization, transverse electric (TE) and transverse magnetic (TM) [32, 50, 51]. The equations of motion for TE-modes in a dynamical rectangular cavity are equivalent to the equations of motion for a scalar field with

*Electronic address: Marcus.Ruser@physics.unige.ch

(time-dependent) Dirichlet boundary conditions [33, 37]. More complicated boundary conditions, so-called generalized Neumann boundary conditions, emerge when studying TM-modes [32, 50]. In most of the works cited above only TE-polarizations are treated. For recent work dealing also with TM-polarizations see [37, 52].

The aim of the present work is to study photon creation in a vibrating three-dimensional cavity fully numerically taking the intermode coupling into account. We show that the equations of motion describing the dynamics of the transverse electric modes (TE) in a dynamical rectangular cavity correspond to the equations of motion for a massive scalar field on a time-dependent interval (one-dimensional cavity). Thereby the wave number of the TE-modes associated with the non-dynamical cavity dimensions is identified with the mass of the scalar field. Creation of TE-polarized photons can then be studied with a formalism presented and tested for a massless scalar field in a one-dimensional cavity in [53, 54]. Even though the method of [53, 54] is valid for a variety of boundary conditions it is not directly applicable to generalized Neumann boundary conditions which involve a time-derivative appearing when studying TM-modes. For other recent numerical work see also [55, 56, 57].

The paper is organized as follows. In section II we present the equations of motion for TE-modes in a three-dimensional rectangular cavity and show that they correspond to the equations of motion for a massive scalar field in a one-dimensional cavity. The formalism for studying the dynamical Casimir effect for a massive scalar field on a time-dependent interval numerically is reviewed in section III. Some analytical results obtained for TE-mode photons are summarized in section IV. We present and interpret the numerical results in section V and discuss their consequences for photon creation in three-dimensional vibrating cavities in section VI. We conclude in section VII and discuss some details about the numerics in the appendix.

II. EQUATIONS OF MOTION FOR TE-MODES IN A RECTANGULAR DYNAMICAL CAVITY

The dynamics of the transverse electric modes (TE-modes) inside a rectangular ideal (i.e. perfectly conducting) cavity of dimensions $\{(0, l_x), (0, l_y), (0, l_z)\}$ is described by the wave (Klein-Gordon) equation¹

$$[\partial_t^2 - \Delta]\Phi(t, \mathbf{x}) = 0 \quad (1)$$

with the massless scalar field $\Phi(t, \mathbf{x})$ subject to Dirichlet boundary conditions at all walls of the cavity [33, 37].

The x -dimension of the cavity is assumed to be dynamical with the right wall following a prescribed trajectory

$l(t) \equiv l_x(t)$. At any moment in time the field can be expanded as

$$\Phi(t, \mathbf{x}) = \sum_{\mathbf{n}} q_{\mathbf{n}}(t) \phi_{\mathbf{n}}(t, \mathbf{x}) \quad (2)$$

with canonical variables $q_{\mathbf{n}}(t)$ and functions

$$\begin{aligned} \phi_{\mathbf{n}}(t, \mathbf{x}) &= \sqrt{\frac{2}{l(t)}} \sin\left[\frac{n_x \pi}{l(t)} x\right] \sqrt{\frac{2}{l_y}} \sin\left[\frac{n_y \pi}{l_y} y\right] \\ &\times \sqrt{\frac{2}{l_z}} \sin\left[\frac{n_z \pi}{l_z} z\right] \end{aligned} \quad (3)$$

ensuring Dirichlet boundary conditions at the positions of the cavity walls [33]. The functions $\phi_{\mathbf{n}}(t, \mathbf{x})$ form an orthonormal and complete set of instantaneous eigenfunctions of the Laplacian Δ with time-dependent eigenvalues

$$\Omega_{\mathbf{n}}(t) = \pi \sqrt{\left(\frac{n_x}{l(t)}\right)^2 + \left(\frac{n_y}{l_y}\right)^2 + \left(\frac{n_z}{l_z}\right)^2}. \quad (4)$$

Each field mode is labeled by three integers $n_x, n_y, n_z = 1, 2, \dots$ for which we use the abbreviation $\mathbf{n} = (n_x, n_y, n_z)$.

Inserting the expansion (2) into the field equation (1), multiplying it with $\phi_{\mathbf{m}}(t, \mathbf{x})$ and integrating over the spatial dimensions leads to the equation of motion for the canonical variables $q_{\mathbf{n}}(t)$ [33]:

$$\begin{aligned} \ddot{q}_{\mathbf{n}}(t) + \Omega_{\mathbf{n}}^2(t) q_{\mathbf{n}}(t) + 2 \sum_{\mathbf{m}} M_{\mathbf{mn}}(t) \dot{q}_{\mathbf{m}}(t) \\ + \sum_{\mathbf{m}} [\dot{M}_{\mathbf{mn}}(t) - N_{\mathbf{nm}}(t)] q_{\mathbf{m}}(t) = 0. \end{aligned} \quad (5)$$

The time-dependent coupling matrices $M_{\mathbf{nm}}(t)$ and $N_{\mathbf{nm}}(t)$ are given by [33]

$$\begin{aligned} M_{\mathbf{nm}} &= \int_0^{l(t)} dx \dot{\phi}_{\mathbf{n}} \phi_{\mathbf{m}} \\ &= \frac{\dot{l}(t)}{l(t)} \begin{cases} (-1)^{n_x+m_x} \frac{2n_x m_x}{m_x^2 - n_x^2} \delta_{n_y m_y} \delta_{n_z m_z} & \text{if } n_x \neq m_x \\ 0 & \text{if } n_x = m_x \end{cases} \end{aligned} \quad (6)$$

and

$$N_{\mathbf{nm}} = \sum_{\mathbf{k}} M_{\mathbf{nk}} M_{\mathbf{mk}}. \quad (7)$$

During the dynamics of the mirror the time evolution of a field mode \mathbf{n} may be coupled to (even infinite many) other modes \mathbf{m} via the time-dependent coupling matrix $M_{\mathbf{nm}}(t)$. In Eq. (5) for a given mode (n_x, n_y, n_z) the coupling matrix (6) yields couplings of $q_{(n_x, n_y, n_z)}$ to $q_{(m_x, n_y, n_z)}$ and $\dot{q}_{(m_x, n_y, n_z)}$, i.e. only summations over m_x appear. Modes with different quantum numbers in the y - and z - directions are not coupled and the quantum numbers corresponding to the non-dynamical dimensions

¹ We are using units with $\hbar = c = 1$.

enter the equations of motion only globally. Therefore we can identify $q_n(t) \equiv q_{(n_x, n_y, n_z)}(t)$ and

$$\Omega_n(t) \equiv \Omega_{(n_x, n_y, n_z)}(t) = \sqrt{\left[\frac{n\pi}{l(t)}\right]^2 + k_{\parallel}^2} \quad (8)$$

with $n \equiv n_x$ and the wave number

$$k_{\parallel} = \pi \sqrt{\left(\frac{n_y}{l_y}\right)^2 + \left(\frac{n_z}{l_z}\right)^2} \quad (9)$$

associated with the non-dynamical cavity dimensions.

Because all summations over $\mathbf{m} = (m_x, m_y, m_z)$ involving the coupling matrix (6) reduce to summations over a single quantum number m , Eq. (5) is equivalent to the differential equation describing a real massive scalar field on a time-dependent interval $[0, l(t)]$ (one-dimensional cavity) when k_{\parallel} is identified with the mass of the field [54]. As pointed out in [37] the number of created TE-mode photons equals the number of created Dirichlet scalar particles in a three-dimensional cavity. Consequently, the number of TE-mode photons created in a three-dimensional cavity equals the number of scalar particles of “mass” k_{\parallel} created in a one-dimensional cavity $[0, l(t)]$. Photon production in TE-modes in a three-dimensional cavity can therefore be studied numerically with the formalism presented in [53, 54].

III. THE FORMALISM

Quantization is achieved by replacing the set of classical canonical variables $\{q_n, p_m\}$ with the corresponding operators $\{\hat{q}_n, \hat{p}_m\}$ and demanding the usual equal-time commutation relations. Furthermore, the Heisenberg picture is adopted from now on. The relation between the canonical variable q_n and the canonical momentum is given by $p_n = \dot{q}_n + \sum_m q_m M_{mn}$. Assuming that the cavity is at rest for times $t \leq 0$ the coupling matrix vanishes and equation (5) reduces to the equation of a harmonic oscillator with constant frequency $\Omega_n^0 \equiv \Omega_n(t \leq 0)$. Consequently

$$\hat{q}_n(t \leq 0) = \frac{1}{\sqrt{2\Omega_n^0}} \left[\hat{a}_n e^{-i\Omega_n^0 t} + \hat{a}_n^{\dagger} e^{i\Omega_n^0 t} \right] \quad (10)$$

with frequency

$$\Omega_n^0 = \frac{1}{l_0} \sqrt{(n\pi)^2 + M^2} \quad (11)$$

where $l_0 = l(0)$ and we have introduced the dimensionless “mass parameter” $M = l_0 k_{\parallel}$. The time-independent annihilation and creation operators $\hat{a}_n, \hat{a}_n^{\dagger}$ associated with the particle notion for $t \leq 0$ are subject to the commutation relations

$$[\hat{a}_n, \hat{a}_m] = [\hat{a}_n^{\dagger}, \hat{a}_m^{\dagger}] = 0, \quad [\hat{a}_n, \hat{a}_m^{\dagger}] = \delta_{nm}. \quad (12)$$

The initial vacuum state $|0, t \leq 0\rangle$ is defined by

$$\hat{a}_n |0, t \leq 0\rangle = 0 \quad \forall n. \quad (13)$$

When the cavity dynamics is switched on at $t = 0$ and the wall follows the prescribed trajectory $l(t)$ field modes are coupled due to the non-vanishing coupling matrix M_{nm} . To account for the coupling, the operator \hat{q}_n may be expanded as [54]

$$\hat{q}_n(t \geq 0) = \sum_m \frac{1}{\sqrt{2\Omega_m^0}} \left[\hat{a}_m \epsilon_n^{(m)}(t) + \hat{a}_m^{\dagger} \epsilon_n^{(m)*}(t) \right] \quad (14)$$

with complex functions $\epsilon_n^{(m)}(t)$ satisfying Eq. (5). If the motion ceases and the wall is at rest again for $t \geq t_1$ the operator $\hat{q}_n(t \geq t_1)$ takes the form ²

$$\hat{q}_n(t \geq t_1) = \frac{1}{\sqrt{2\Omega_n^1}} \left[\hat{A}_n e^{-i\Omega_n^1(t-t_1)} + \hat{A}_n^{\dagger} e^{i\Omega_n^1(t-t_1)} \right] \quad (15)$$

with $\Omega_n^1 \equiv \Omega_n(t \geq t_1)$ and annihilation and creation operators $\hat{A}_n, \hat{A}_n^{\dagger}$ corresponding to the particle notion for $t \geq t_1$. The final vacuum state $|0, t \geq t_1\rangle$ is defined by

$$\hat{A}_n |0, t \geq t_1\rangle = 0 \quad \forall n. \quad (16)$$

The initial state particle operators $\hat{a}_n, \hat{a}_n^{\dagger}$ are linked to the final state particle operators $\hat{A}_n, \hat{A}_n^{\dagger}$ by the Bogoliubov transformation

$$\hat{A}_n = \sum_m \left[\mathcal{A}_{mn}(t_1) \hat{a}_m + \mathcal{B}_{mn}^*(t_1) \hat{a}_m^{\dagger} \right] \quad (17)$$

and the number of particles (photons) created in a mode n during the motion of the wall is given by the expectation value of the number operator $\hat{A}_n^{\dagger} \hat{A}_n$ associated with the particle notion for $t \geq t_1$ with respect to the initial vacuum state $|0, t \leq 0\rangle$:

$$\begin{aligned} N_n(t_1) &= \langle 0, t \leq 0 | \hat{A}_n^{\dagger} \hat{A}_n | 0, t \leq 0 \rangle \\ &= \sum_m |\mathcal{B}_{mn}(t_1)|^2. \end{aligned} \quad (18)$$

The total number of created particles as the sum of $N_n(t_1)$ over all quantum numbers n

$$N(t_1) = \sum_n N_n(t_1) = \sum_n \sum_m |\mathcal{B}_{mn}(t_1)|^2 \quad (19)$$

is in general ill-defined and requires appropriate regularization. This can be done most easily by introducing an explicit frequency cut-off which also simulates non-ideal boundary conditions for high frequency modes [14]. As a

² Here $l(t_1) = l_1$ is assumed to be arbitrary. For an oscillating cavity, however, it is natural to consider times t_1 after which the dynamical wall has returned to its initial position.

matter of course, such a frequency cut-off has to be used in the numerical simulations.

In order to calculate $\mathcal{B}_{mn}(t_1)$ we introduce auxiliary functions $\xi_n^{(m)}(t)$ and $\eta_n^{(m)}(t)$ via [54]

$$\xi_n^{(m)}(t) = \epsilon_n^{(m)}(t) + \frac{i}{\Omega_n^0} \left[\dot{\epsilon}_n^{(m)}(t) + \sum_k M_{kn}(t) \epsilon_k^{(m)}(t) \right], \quad (20)$$

$$\eta_n^{(m)}(t) = \epsilon_n^{(m)}(t) - \frac{i}{\Omega_n^0} \left[\dot{\epsilon}_n^{(m)}(t) + \sum_k M_{kn}(t_1) \epsilon_k^{(m)}(t) \right]. \quad (21)$$

Using the second order differential equation (5) for $\epsilon_n^{(m)}(t)$ it is easily shown that those functions satisfy the following system of coupled first-order differential equations [54]:

$$\begin{aligned} \dot{\xi}_n^{(m)}(t) &= -i \left[a_{nn}^+(t) \xi_n^{(m)}(t) - a_{nn}^-(t) \eta_n^{(m)}(t) \right] \\ &\quad - \sum_k \left[c_{nk}^-(t) \xi_k^{(m)}(t) + c_{nk}^+(t) \eta_k^{(m)}(t) \right], \quad (22) \end{aligned}$$

$$\begin{aligned} \dot{\eta}_n^{(m)}(t) &= -i \left[a_{nn}^-(t) \xi_n^{(m)}(t) - a_{nn}^+(t) \eta_n^{(m)}(t) \right] \\ &\quad - \sum_k \left[c_{nk}^+(t) \xi_k^{(m)}(t) + c_{nk}^-(t) \eta_k^{(m)}(t) \right] \quad (23) \end{aligned}$$

with

$$a_{nn}^\pm(t) = \frac{\Omega_n^0}{2} \left\{ 1 \pm \left[\frac{\Omega_n(t)}{\Omega_n^0} \right]^2 \right\}, \quad (24)$$

$$c_{kn}^\pm(t) = \frac{1}{2} \left[M_{nk}(t) \pm \frac{\Omega_n^0}{\Omega_k^0} M_{kn}(t) \right]. \quad (25)$$

For the coupling matrix (6) one finds in particular

$$c_{kn}^\pm(t) = -\frac{\dot{l}(t)}{l(t)} (-1)^{k+n} \frac{kn}{n^2 - k^2} \left[1 \mp \frac{\Omega_n^0}{\Omega_k^0} \right] \quad (26)$$

if $n \neq k$ and $c_{nn}^\pm(t) = 0$. The advantage of this system of first-order differential equations relies on the fact that, besides the time-dependent frequency $\Omega_n(t)$, only the coupling matrix M_{nk} enters but neither its square N_{nk} nor its time derivative \dot{M}_{nk} .

By matching Eq. (14) with Eq. (15) for $\hat{q}_n(t)$ and the corresponding expressions for $\hat{p}_n(t)$ at $t = t_1$ one finds the relations [54]

$$\mathcal{A}_{mn}(t_1) = \frac{1}{2} \sqrt{\frac{\Omega_n^1}{\Omega_n^0}} \left[\Delta_n^+(t_1) \xi_n^{(m)}(t_1) + \Delta_n^-(t_1) \eta_n^{(m)}(t_1) \right], \quad (27)$$

$$\mathcal{B}_{mn}(t_1) = \frac{1}{2} \sqrt{\frac{\Omega_n^1}{\Omega_n^0}} \left[\Delta_n^-(t_1) \xi_n^{(m)}(t_1) + \Delta_n^+(t_1) \eta_n^{(m)}(t_1) \right] \quad (28)$$

with

$$\Delta_n^\pm(t) = \frac{1}{2} \left[1 \pm \frac{\Omega_n^0}{\Omega_n(t)} \right]. \quad (29)$$

Demanding that the field be in its vacuum state $|0, t \leq 0\rangle$ as long as the mirror is at rest implies $\mathcal{A}_{mn}(0) = \delta_{mn}$ and $\mathcal{B}_{mn}(0) = 0$. Accordingly the initial conditions for $\xi_n^{(m)}(t)$ and $\eta_n^{(m)}(t)$ read

$$\xi_n^{(m)}(0) = 2\delta_{mn}, \quad \eta_n^{(m)}(0) = 0. \quad (30)$$

By means of Eq. (28) the number of created massive scalar particles, or equivalently the number of created TE-mode photons, at time $t = t_1$ can now be calculated by solving the system of differential equations formed by Eqs. (22) and (23) numerically using standard numerics. For this we truncate the infinite sums by introducing a cut-off quantum number k_{\max} to make the system of differential equations suitable for numerical treatment. The system is evolved up to a final time t_{\max} and the particle number (18) is calculated for several times in between, i.e. we interpret t_1 as a continuous variable such that the particle number (18) becomes a continuous function of time³. Consequently, the stability of the numerical results has to be guaranteed which means that for the lowest modes n the numerical values for $N_n(t)$ remain practically unchanged under variation of k_{\max} . More details regarding the numerics are collected in the appendix.

IV. KNOWN ANALYTICAL RESULTS

In what follows, we consider the periodic trajectory

$$l(t) = l_0 [1 + \epsilon \sin(\omega t)] \quad , \quad \epsilon \ll 1, \quad (31)$$

for which it was found in [33] that two modes l and k are coupled whenever one of the conditions given by

$$\omega = |\Omega_l^0 \pm \Omega_k^0| \quad (32)$$

is satisfied⁴. In a resonantly vibrating cavity $\omega = 2\Omega_n^0$ with not one of those conditions fulfilled the number of TE-mode photons created in the resonant mode n increases exponentially in time [33]:

$$N_n(t) = \sinh^2(n \gamma_n \epsilon t) \quad \text{with} \quad \gamma_n = \frac{n}{2\Omega_n^0} \left(\frac{\pi}{l_0} \right)^2. \quad (33)$$

³ Potential problems inherent in this procedure like the appearance of discontinuities in the velocity of the mirror motion occurring when calculating the particle number for times t for which $\dot{l}(t) \neq 0$ are discussed in [54] in detail. We come back to this in section V.

⁴ Here and in the following we have translated the results for three-dimensional cavities to the case of massive scalar particles according to Eq. (8).

By means of multiple scale analysis the authors of [33] also studied the resonance case $\omega = 2\Omega_n^0$ with two coupled modes n and k satisfying

$$3\Omega_n^0 = \Omega_k^0. \quad (34)$$

For the particular case $n = 1$ and $k = 5$ analytical expressions for the number of TE-mode photons are derived in [33]. Given a mode n we can couple it to a particular mode k by tuning the mass M (or equivalently k_{\parallel}) such that the condition (34) is fulfilled. It is important to note that coupling between modes does occur even if Eq. (32) is detuned, i.e. if Eq. (32) is satisfied by the frequencies Ω_k^0 and Ω_l^0 only approximately. The particular case of two modes n and k satisfying

$$(3 + \kappa)\Omega_n^0 = \Omega_k^0 \quad (35)$$

without additional couplings to higher modes was studied in [36]. For sufficiently small κ (i.e., $\kappa < \epsilon$) the two modes n and k are still resonantly coupled and the number of particles produced in both modes increasing exponentially with time.

V. NUMERICAL RESULTS

A. Preliminary remarks

In [53, 54] we have employed the same formalism to study the creation of massless scalar particles in a one-dimensional vibrating cavity numerically. In this case the numerical results agree with analytical predictions obtained under the assumption $\epsilon \ll 1$ demonstrating the reliability of the numerics. The extension to massive scalar fields is straightforward. We set $l_0 = 1$, i.e. all physical quantities with dimensions are measured with respect to the length scale l_0 and dimensionless quantities are used throughout. The amplitude of the oscillations is fixed to $\epsilon = 0.001$ guaranteeing accordance between the numerical results and the analytical predictions in the massless case [53, 54].

As mentioned before, we calculate the particle number for arbitrary times even though the analytical expressions we are comparing the numerical results with are valid only for times after which the dynamical wall has returned to its initial position. In [53] it is shown that (for a vibrating cavity) this leads to oscillations in the particle number which are of negligibly small amplitude when the amplitude of the cavity oscillations itself is small ($\epsilon \ll 1$). We will briefly come back to this question later on. Furthermore, when calculating the particle number at times t for which $\dot{l}(t) \neq 0$ the used particle definition requires a matching of the solutions to expressions corresponding to the static cavity $\dot{l}(t) = 0$. This discontinuity in the velocity of the mirror trajectory may give rise to spurious contributions to the total particle number. The cut-off k_{\max} automatically ensures that the total particle number remains finite because it automatically smoothes the

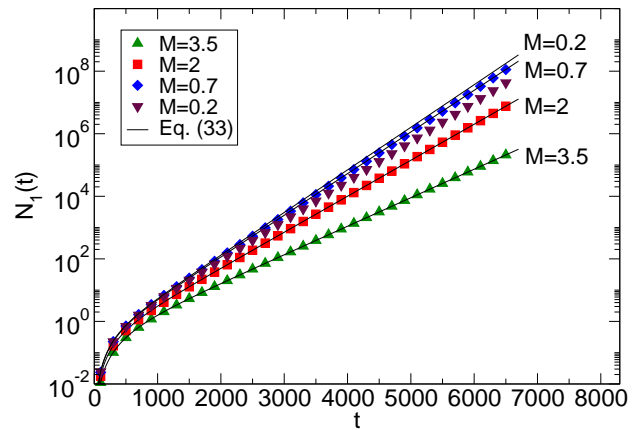


FIG. 1: (color online) Number of particles created in the resonance mode $n = 1$ for mass parameters $M = 0.2, 0.7, 2$, and 3.5 in comparison with the analytical prediction (33).

motion. For a more detailed discussion see [54] where it is shown that the influence of such discontinuities is negligibly small in the case of a cavity vibrating with sufficiently small amplitudes ($\epsilon = 0.001$). (For a detailed discussion of how the initial discontinuity in the mirror motion (31) affects the particle creation see also [53].) The numerical results which are presented and discussed in the following are practically not affected by the above mentioned effects.

B. Main resonance $\omega = 2\Omega_1^0$

In Fig. 1 the number $N_1(t)$ of particles created in the resonant mode $k = 1$ is shown for masses $M = 0.2, 0.7, 2$ and 3.5 and compared to the analytical prediction Eq. (33)⁵. For $M = 0.7, 2$ and 3.5 the numerical results are well described by Eq. (33) which is valid provided that the resonant mode $n = 1$ is not coupled to other modes. In case of the mass $M = 0.2$ the numerical result for $N_1(t)$ disagrees with the analytical prediction (33). This will be discussed in the following in detail. Figure 2 shows the corresponding particle spectra at time $t = 6700$. One infers that for $M = 3.5, 2$ and 0.7 the mode which becomes excited most is indeed the resonant mode $n = 1$. However, also higher modes become excited but the corresponding particle numbers are several orders of magnitude smaller than the number of particles created in the resonant mode. For $M = 0.7$, for example, the mode $k = 3$ is clearly excited. Figure 3 shows the number of particles created in the modes $k = 1, 2$ and 3 for the mass parameter $M = 0.7$ in detail. The difference

⁵ In this section we use the general notion “particles” for massive scalar particles, or equivalently, TE-mode photons. Furthermore we call M the mass of the particle, having in mind that it corresponds to the wave number k_{\parallel} for TE-mode photons.

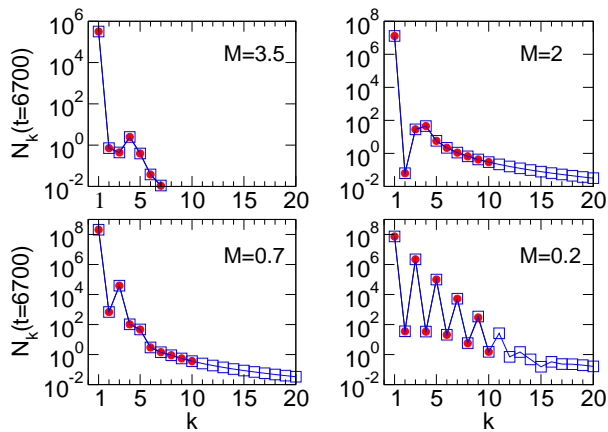


FIG. 2: (color online) Particle spectrum for different mass parameters $M = 3.5, 2, 0.7$ and $M = 0.2$ at time $t = 6700$ corresponding to Fig. 1. The spectra are shown for $k_{\max} = 10$ (dots) and $k_{\max} = 20$ (squares) to demonstrate numerical stability.

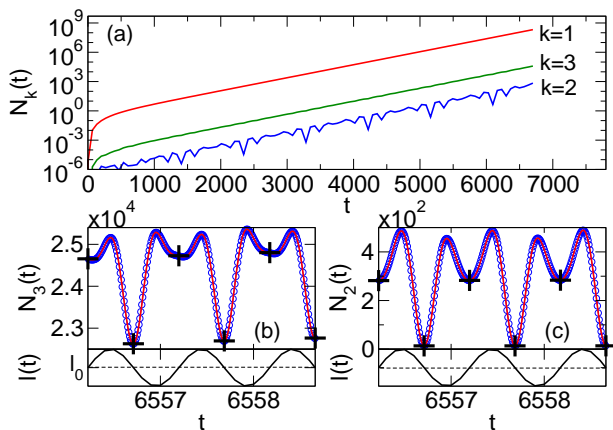


FIG. 3: (color online) (a) Number of particles created in the modes $k = 1, 2$ and 3 for the mass parameter $M = 0.7$ corresponding to the spectra shown in Fig. 2. Part (b) shows $N_3(t)$ and part (c) $N_2(t)$ in each case for the two resolutions $\Delta t = 0.01$ (circles) and $\Delta t = 0.005$ (solid lines). The particle numbers calculated for times at which the mirror has returned to its initial position are accented by “+” and the background motion is shown for comparison as well.

in the numerical values of N_1 and N_3 is so large that the contribution of N_3 to the total particle number is negligible such that $N \simeq N_1$. From Fig. 3 (a) one could conclude that N_2 , i.e. the number of particles created in the mode $k = 2$, behaves in the same way as N_3 but shows superimposed oscillations. However, Figs. 3 (b) and (c) provide a more detailed view on the time evolution of $N_k(t)$ for modes $k = 2$ and 3 . In Fig. 3 (a) the resolution in which the numerical results are shown is not sufficient in order to resolve the details which are visible in Figs. 3 (b) and (c). These high resolution pictures reveal that N_3 increases exponentially in time with oscillations superimposed on an average particle number

whereas N_2 itself oscillates strongly with an amplitude negligibly small compared to N_1 .

The small scale oscillations in the particle numbers are correlated with the periodic motion of the mirror which we have depicted in Figs. 3 (b) and (c) as well. But one infers that the particle numbers show oscillations also when the expectation value (18) is calculated only for times at which the mirror has returned to its initial position l_0 . Therefore the oscillations cannot be traced back exclusively to the fact that Eq. (18) is calculated for arbitrary times which may be considered as unphysical.

The observation that also higher modes become excited (even though they are very much suppressed) is explained by the fact that two modes k and l are coupled even if Eq. (32) is not exactly satisfied by the two frequencies Ω_k^0 and Ω_l^0 . For $M = 0.7$ the equation $3\Omega_1^0 = \Omega_k^0$ has no solution for integer k . Thus taking Eq. (32) as an exact equation only the resonant mode should become excited and particle creation should take place in the mode $n = 1$ exclusively. Inserting $M = 0.7$ one finds the solution $k \sim 3.07$ which is apparently close enough to the integer value $k = 3$ to excite that mode. For smaller values of M the solution of $3\Omega_1^0 = \Omega_k^0$ approaches the value $k = 3$ and one has to expect that for sufficiently small values of M the mode coupling becomes again so strong that Eq. (33) does no longer describe the numerical results. This is the case for $M = 0.2$ yielding $k \sim 3.005$ for which a strong coupling between the modes $n = 1$ and $k = 3$ occurs. Furthermore, from Eq. (32) and the coupling of $n = 1$ and $k = 3$ follows $2\Omega_1^0 + \Omega_3^0 = \Omega_l^0$ which has $l \sim 5.004$ as solution, i.e. the mode $k = 3$ is coupled to the mode $l = 5$. In the same way the mode 5 is coupled to the mode $l = 7$. Thus interpreting Eq. (32) as $\omega \simeq |\Omega_k^0 \pm \Omega_l^0|$ explains the numerically computed particle spectrum (cf. Fig. 2) which shows similar features as the spectrum obtained for the massless case (cf Fig. 4 (b) of [53]). One observes that also even modes become excited (like also for $M = 0.7$) which is not the case for $M = 0$ [53]. These modes are dragged by the strongly excited modes (odd modes) and rapidly oscillate (like N_2 for $M = 0.7$) with an amplitude several orders of magnitude smaller compared to N_1 , N_3 and N_5 . In Fig. 4 we show the number of particles created in the modes $k = 1$ to 5 for $M = 0.2$ to illustrate the just-stated. As for $M = 0.7$ the number of particles created in the odd modes increases exponentially showing oscillations superimposed on an average particle number while the number of particles created in the even modes $k = 2$ and $k = 4$ consists of oscillations only with amplitudes much smaller compared to the number of particles created in the odd modes. As in Fig. 3 the strongly oscillating behavior of the particle numbers for even modes is visible in high time resolution only [part (c) of Fig. 4].

The fact that mode coupling occurs even if Eq. (32) is not satisfied exactly is well known. We can rewrite the expression $3\Omega_n \simeq \Omega_k^0$ to get $(3 + \kappa)\Omega_n^0 = \Omega_k^0$ [Eq. (35)]. As mentioned at the end of the former section it was shown for this case in [36] that for sufficiently small κ

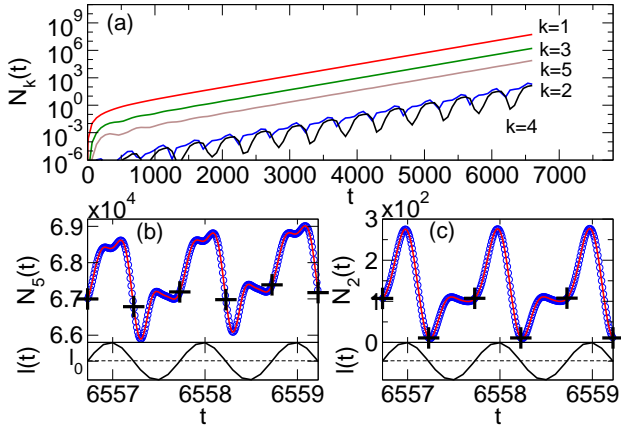


FIG. 4: (color online) (a) Number of particles created in the modes $k = 1, 2, 3, 4$ and 5 for the mass parameter $M = 0.2$ corresponding to the spectrum shown in Fig. 2. Part (b) shows $N_5(t)$ and part (c) $N_2(t)$ in each case for the two resolutions $\Delta t = 0.01$ (circles) and $\Delta t = 0.005$ (solid lines).

the modes n and k are still resonantly coupled, provided that no coupling to higher modes exists. However, the case of two detuned coupled modes does not apply to the scenario discussed here. Decreasing the detuning, i.e. reducing the value of M , does not only strengthen the coupling between the modes $n = 1$ and $k = 3$ which would lead to an exponential growth of the particle number in both modes but also enhances the coupling strength to higher modes $k = 5, 7, \dots$ because the frequency spectrum becomes equidistant as $M \rightarrow 0$ (cf, e.g., [15, 53]). The convergence of the numerical results towards the analytical expressions for the massless case is demonstrated below.

To study in more detail how the number of produced particles depends on the mass we performed numerical simulations for a wide range of values for M . The results are summarized in Fig. 5 in a "mass spectrum" where the number of particles created in the resonant mode $N_1(t = 2000)$ is plotted as a function of M and compared to the analytical prediction Eq. (33). Particular values of M for which Eq. (32) gives integer solutions, i.e. exact (un-detuned) intermode coupling, are marked by arrows and the values of M are indicated. Numerical results for these values are not included in the spectrum. Cases with exact coupling will be discussed later on.

The numerical values for N_1 perfectly agree with the analytical prediction (33) for values of M larger than roughly $M = 0.6$. For masses smaller than this threshold value the number of created particles is smaller compared to the analytical prediction. The mass spectrum exhibits a maximum at around $M \sim 0.4$, i.e. particle production in the resonant mode is most efficient for this particular mass. When $M < 0.4$ the number of created particles drops down and approaches the $M = 0$ result. The appearance of a maximum in the mass spectrum is clear from the above discussion. For the particular value $M = 0.4$ the equation $3\Omega_1^0 = \Omega_k^0$ leads to a value

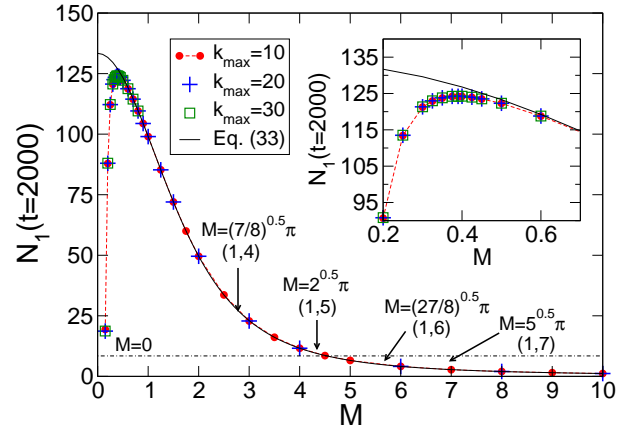


FIG. 5: (color online) Number of particles created in the resonance mode $n = 1$ at time $t = 2000$ as a function of the mass parameter M . The solid line shows the analytical prediction Eq. (33). Arrows pointing towards particular mass values of M mark masses for which Eq. (33) is not valid because of exact intermode coupling. The coupled modes are given in brackets $[(1, k)]$. No numerical results are shown in the plot for those cases. Most of the numerical results are shown for different values of the cut-off k_{\max} to underline stability.

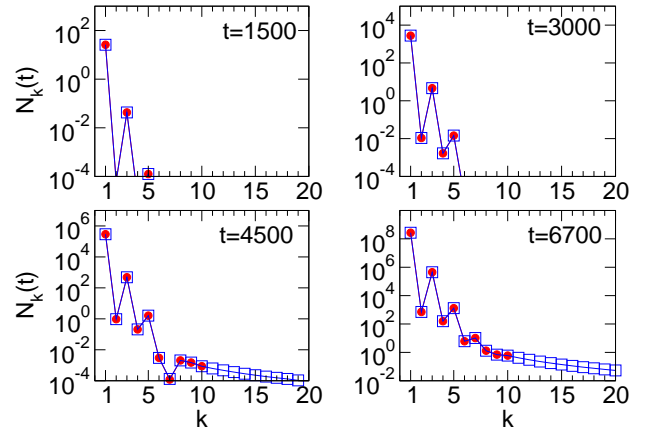


FIG. 6: (color online) Particle spectra for mass parameter $M = 0.4$ at times $t = 1500, 3000, 4500$ and 6700 . Each spectrum is shown for values $k_{\max} = 10$ (dots) and $k_{\max} = 20$ (squares) to indicate numerical stability.

$k = 3.02$ which is close enough to the integer solution $k = 3$ to couple this mode strongly to the resonant mode but on the other hand coupling to higher modes is still suppressed. Figure 6 shows the particle spectrum obtained for $M = 0.4$ for different times and in Fig. 7 the time evolution of the number of particles created in the modes $k = 1, 2, 3$ and 4 is plotted. For the even modes $k = 2$ and 4 the same oscillating behavior is observed as for $M = 0.7$ and $M = 0.2$. The coupling of the mode $k = 3$ to the mode $n = 1$ results in a damping of the resonant mode and consequently the number of particles produced in the mode $n = 1$ is smaller than the value predicted by Eq. (33).

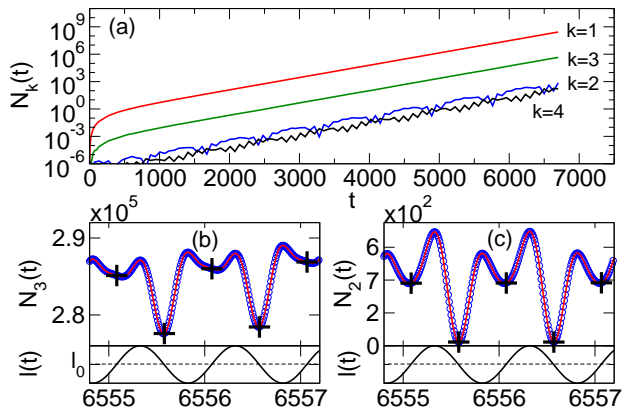


FIG. 7: (color online) (a) Number of particles created in the modes $k = 1, 2, 3$ and 4 for the mass parameter $M = 0.4$ corresponding to the spectra shown in Fig. 6. Part (b) shows $N_3(t)$ and part (c) $N_2(t)$ in each case for the two resolutions $\Delta t = 0.01$ (circles) and $\Delta t = 0.005$ (solid lines).

For increasing masses larger than $M = 0.4$ the excitation of higher modes becomes more and more suppressed (cf Fig. 2). Accordingly the numerical results match the analytical expression (33) predicting that the number of created particles decreases with increasing mass. Decreasing the mass below $M = 0.4$ enhances the strength of the intermode coupling which results in a damping of the resonant mode $n = 1$. Consequently the number of particles produced in the mode $n = 1$ (and also the total particle number) is smaller than predicted analytically. When studying the limit $M \rightarrow 0$ the numerical results should converge towards the well known results for the massless case where all odd modes are coupled [15, 53]. This is demonstrated in Fig. 8 where the total particle number and the number of particles created in the resonant mode $n = 1$ are depicted for $M = 0.2, 0.15, 0.1$ and 0.05 up to $t = 500$ and compared with the analytical predictions for $M = 0$ [15] (see also Figs. 4 (a) and (b) of [53]). While for $M = 0.2$ the total particle number $N(t)$ is still mainly given by $N_1(t)$ a divergency between $N(t)$ and $N_1(t)$ starts to become visible for $M = 0.15$, i.e. the influence of the intermode coupling gains importance. For $M = 0.1$ the numerical results are close to the analytical $M = 0$ -results and are practically identical to them for $M = 0.05$.

We now turn to cases with exact coupling between two modes. As already mentioned above exact coupling of modes takes place if the conditional equation (32) has integer solutions. In particular, exact coupling between two modes n and k occurs if Eq. (34) is satisfied. In [33] the authors derived analytical expressions (Eqs. (54) and (55) of [33]) for the case that the TE-mode $\Omega_{(1,1,1)}^0$ (resonant mode) is coupled to the mode $\Omega_{(5,1,1)}^0$, i.e. $3\Omega_{(1,1,1)}^0 = \Omega_{(5,1,1)}^0$ is fulfilled. This particular case is equivalent to the coupling of the massive modes $n = 1$ and $k = 5$ if $M = \sqrt{2}\pi$ ($l_0 = 1$). Figure 9 shows the numerically obtained particle spectrum

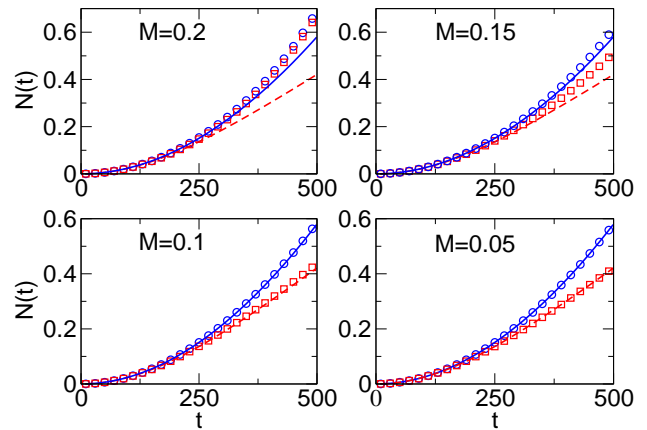


FIG. 8: (color online) Total particle number N (circles) and number of particles created in the mode $k = 1$ N_1 (squares) for mass parameters $M = 0.2, 0.15, 0.1$ and 0.05 together with the analytical predictions for the massless case Eq. (6.5) (dashed line) and Eq. (6.10) (solid line) of [15] to demonstrate the convergence of the solutions towards the $M = 0$ case (see also Fig. 4 of [53]). The cut-off parameter $k_{\max} = 30$ was used in the simulations.

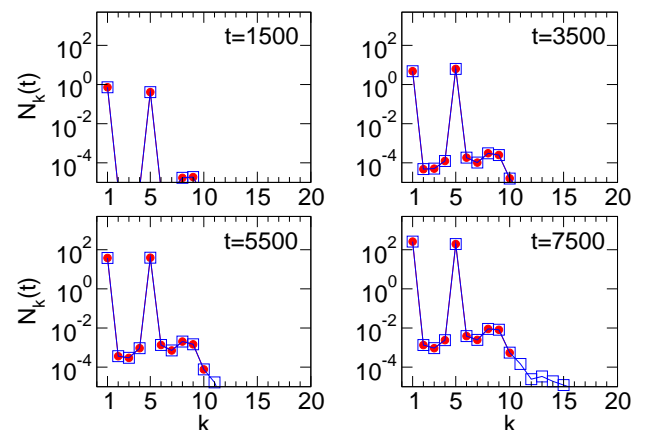


FIG. 9: (color online) Particle spectra for $\omega = 2\Omega_1^0$ and mass parameter $M = \sqrt{2}\pi$ yielding exact coupling between the modes $n = 1$ and $k = 5$. Dots correspond to $k_{\max} = 10$ and squares to $k_{\max} = 20$.

at four different times. The cut-off parameter $k_{\max} = 20$ guarantees stability of the numerical results. The numerical simulations confirm the prediction that practically only the modes $n = 1$ and $k = 5$ become excited and particles are produced exclusively in the two coupled modes. Thereby the rate of particle creation is equal for the two modes. In Fig. 10 we show the numerical results for $N_1(t)$ and $N_5(t)$ and compare them with the analytical expressions Eq. (54) and Eq. (55) of [33] derived via multiple scale analysis (MSA). Whereas the numerical results agree quite well with the analytical prediction of [33] for long times, one observes a discrepancy between the numerical results and the analytical predictions for "shorter times" up to $t \sim 3000$ ($\epsilon\pi t = 3\pi$). For

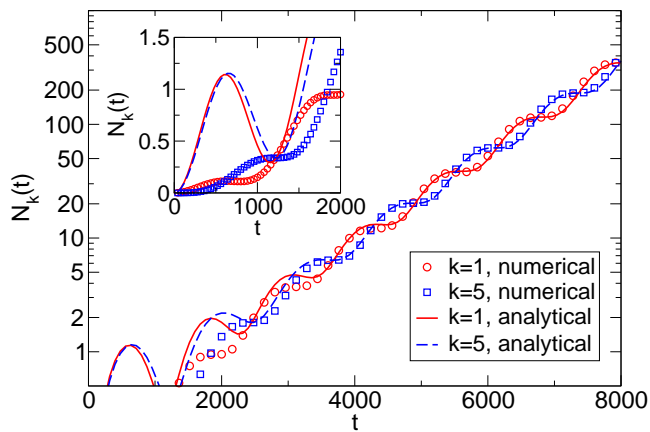


FIG. 10: (color online) Number of particles created in the modes $n = 1$ and $k = 5$ for $\omega = 2\Omega_1^0$ and $M = \sqrt{2}\pi$ corresponding to the particle spectra depicted in Fig. 9. The numerical results are compared to the analytical predictions Eq. (54) [solid line] and Eq. (55) [dashed line] of [33]. The numerical results shown correspond to the cut-off parameter $k_{\max} = 20$ which guarantees stability.

long times, the analytical predictions nicely reproduce the large scale oscillations in the exponentially increasing particle numbers. For times up to $t \sim 500$, the numerically calculated particle numbers grow with a much smaller rate than predicted by Eqs. (54) and (55) of [33]. Furthermore, the analytical expressions predict that for “short times” N_1 and N_5 increase with the same rate whereas from the numerical simulations we find that the production of particles in the mode $k = 5$ sets in after the production of particles in the $n = 1$ -mode. Apart from the differences for short times the numerical results are well described by the analytical predictions of [33]. The discrepancy between the analytical predictions and the numerical results for short times is due to the fact that the MSA analysis in [33] only considers the resonant coupled modes, but for short enough times all modes should be treated on an equal footing [58].

As a second example of exact coupling between two modes we show in Figs. 11 and 12 the numerical results obtained for $M = \sqrt{7/8}\pi$ for which the mode $n = 1$ is coupled to the mode $k = 4$.

Let us discuss another case with exact coupling of two modes which impressively demonstrates that strong coupling between modes k and l occurs even if Eq. (32) is satisfied only approximately. For $M = \sqrt{5}\pi$ equation (32) predicts that the mode $n = 1$ is exactly coupled to the mode $k = 7$ (i.e. $k = 7$ is an integer solution of $3\Omega_1^0 = \Omega_k^0$). The equation $2\Omega_1^0 = \Omega_l^0 - \Omega_7^0$ is not satisfied by an integer l but has the solution $l \sim 12.04$ which is close to the integer $l = 12$. Thus we can expect a coupling of the mode $k = 7$ to the mode $l = 12$. In addition one finds that the equation $2\Omega_1^0 = \Omega_m^0 - \Omega_{12}^0$ has solution $m = 16.96$, i.e. $m \sim 17$, and hence $l = 12$ is coupled to $m = 17$. In the same way the equation $2\Omega_1^0 = \Omega_j^0 - \Omega_{17}^0$ which is solved by $j \sim 21.93$ leads to a coupling between

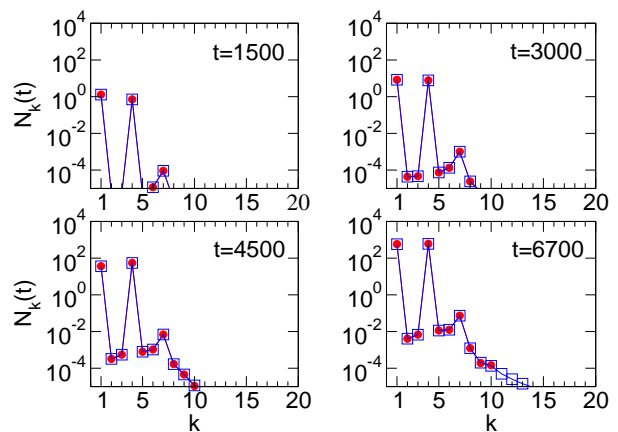


FIG. 11: (color online) Particle spectra for $\omega = 2\Omega_1^0$ and mass parameter $M = \sqrt{7/8}\pi$ yielding exact coupling between the modes $n = 1$ and $k = 4$. Dots correspond to $k_{\max} = 10$ and squares to $k_{\max} = 20$.

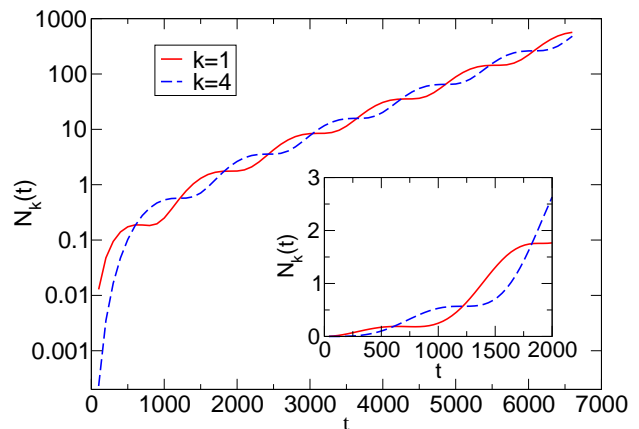


FIG. 12: (color online) Number of particles created in the modes $n = 1$ and $k = 4$ for $\omega = 2\Omega_1^0$ and mass parameter $M = \sqrt{7/8}\pi$ corresponding to the particle spectra depicted in Fig. 11.

the modes $m = 17$ and $j = 22$. Hence from the numerical simulations we expect to find a particle spectrum showing that particle creation takes place in the modes $k = 1, 7, 12, 17$ and 22 . This is demonstrated in Fig. 13 where the numerically evaluated particle spectrum is depicted for times $t = 500, 1000, 1500$ and 2000 . The cut-off parameter $k_{\max} = 50$ ensures numerical stability in the integration range considered⁶. The number of created particles $N_k(t)$ is shown in Fig. 14 for the modes $k = 1, 7$ and 17 .

Without having done a detailed analysis we find, as a reasonable approximation, that a mode l is (strongly)

⁶ From Fig. 13 one observes that also the mode $l = 27$ is weakly coupled. The equation $2\Omega_1^0 = \Omega_l^0 - \Omega_{22}^0$ has the solution $l \sim 26.92$ which explains the excitation of the mode $l = 27$.

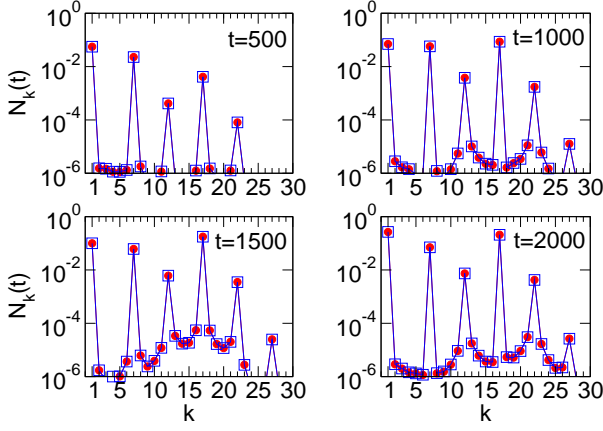


FIG. 13: (color online) Particle spectra for $\omega = 2\Omega_1^0$ and mass parameter $M = \sqrt{5}\pi$. Dots correspond to $k_{\max} = 40$ and squares to $k_{\max} = 50$.

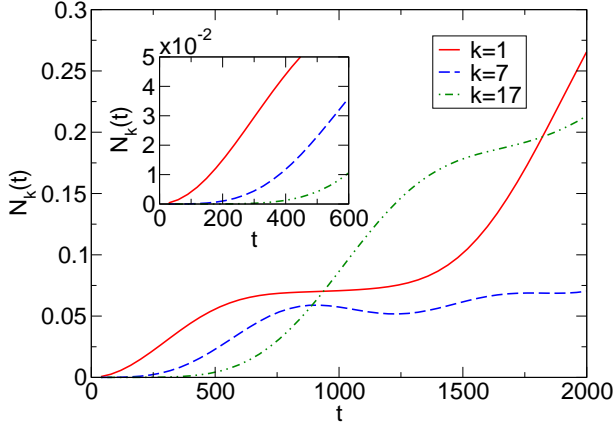


FIG. 14: (color online) Number of particles created in the modes $n = 1$, $k = 7$ and $l = 17$ for $\omega = 2\Omega_1^0$ and mass parameter $M = \sqrt{5}\pi$ corresponding to the particle spectra depicted in Fig. 13.

coupled to a given mode k whenever the ratio $|l - \tilde{l}|/l$ with \tilde{l} denoting the solution of $2\Omega_n^0 = |\Omega_{\tilde{l}}^0 \pm \Omega_k^0|$ is of the order of or smaller than 10^{-3} , i.e. of the order of or smaller than ϵ used in the simulations.

C. Higher resonance $\omega = 2\Omega_2^0$

Now we briefly discuss results obtained for the cavity frequency $\omega = 2\Omega_2^0$. In Fig. 15 we show a numerically calculated mass spectrum similar to the one depicted in Fig. 5. The qualitative behavior is the same as discussed for the main resonance case. As in Fig. 5 results for values of the mass parameter M for which modes are exactly coupled are not included in the spectrum but marked by arrows with the corresponding coupled modes given in brackets. The numerical results again perfectly agree with the analytical prediction (33) for values of

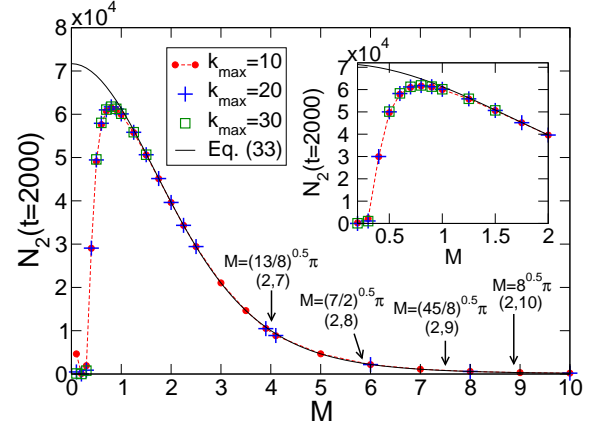


FIG. 15: (color online) Number of particles created in the resonance mode $n = 2$ as function of the mass parameter M . The solid line corresponds to the analytical prediction (33). Note that the first three values in the spectrum are not numerically stable due to an insufficient k_{\max} .

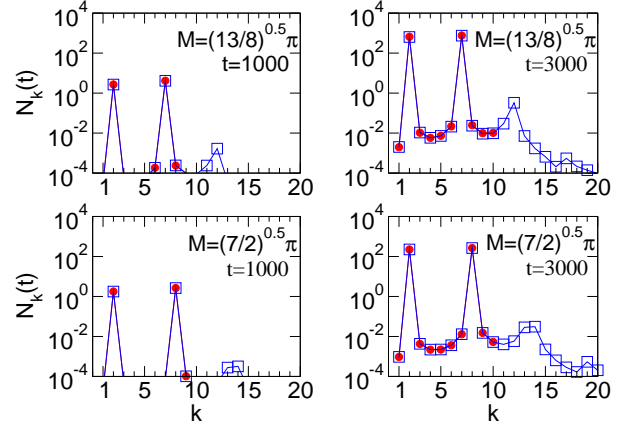


FIG. 16: (color online) Particle spectra for $\omega = 2\Omega_2^0$ and mass parameters $M = \sqrt{13/8}\pi$ and $M = \sqrt{7/2}\pi$.

M larger than a threshold value which is roughly 1.3. The maximum in the particle spectrum appears now for $M \sim 0.8$ and the interpretation of the shape of the mass spectrum is equivalent to the one given for the case $\omega = 2\Omega_1^0$.

In Figs. 16 and 17 we finally show numerical results for the two mass parameters $M = \sqrt{13/8}\pi$ and $M = \sqrt{7/2}\pi$ yielding exact coupling between the modes 2 and 7, respectively, 2 and 8.

VI. PHOTON CREATION IN A THREE-DIMENSIONAL CAVITY

The analogy between massive scalar particles and transverse electric photons in a three-dimensional rectangular cavity outlined in Section II allows to interpret the presented numerical results as follows: Consider a

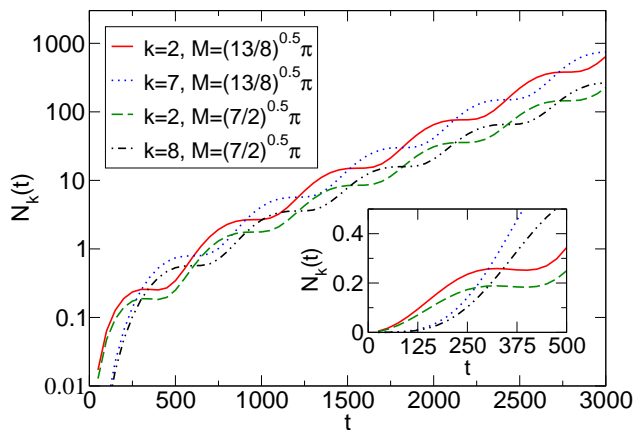


FIG. 17: (color online) Number of particles created in the modes $k = 2$ and 7 for $M = \sqrt{13/8}\pi$, respectively, $k = 2$ and 8 for $M = \sqrt{7/2}\pi$, corresponding to the particle spectra shown in Fig. 16.

three-dimensional rectangular cavity with equally sized non-dynamical dimensions $l_y = l_z \equiv l_{\parallel}$. We parametrize the size of l_{\parallel} in terms of the initial size of the dynamical dimension $l_0 = l_x(0)$ by introducing $\ell = l_{\parallel}/l_0$. If we restrict ourselves for simplicity to the case $n_y = n_z \equiv n_{\parallel}$, the dimensionless mass parameter M reads

$$M = l_0 k_{\parallel} = \sqrt{2} \left(\frac{n_{\parallel} \pi}{\ell} \right). \quad (36)$$

Therefore, for fixed n_{\parallel} , any value of M corresponds to a particular realization, i.e. size ℓ , of the non-dynamical cavity dimensions. We have found that for a particular value M the production of massive scalar particles in the resonant mode is maximal. Consequently it is possible to maximize the production of TE-photons in a three-dimensional rectangular cavity by tuning the size ℓ of the non-dynamical cavity dimensions.

For instance, for $\omega = 2\Omega_1^0$ the creation of massive scalar particles in the resonant mode $n = 1$ is most efficient for $M \sim 0.4$ (cf. Fig. 5). This corresponds to the three-dimensional case with $\omega = 2\Omega_{(1,1,1)}^0$ and $\ell \sim 11$. Hence by designing the three-dimensional cavity such that $l_{\parallel} \sim 11l_0$ the production of TE-mode photons in the resonant mode $(1, 1, 1)$ can be maximized. In order to maximize the creation of TE-photons in the mode $(1, 2, 2)$ when $\omega = 2\Omega_{(1,2,2)}^0$ the size l_{\parallel} of the non-dynamical dimensions has to be doubled, i.e. $l_{\parallel} \sim 22l_0$. For $\omega = 2\Omega_2^0$ we have found that the maximum in the mass spectrum is at $M \sim 0.8$ [cf Fig. 15]. Accordingly, the production of TE-photons of frequency $\Omega_{(2,1,1)}^0$ under resonance conditions is maximal in a cavity of dimensions $l_{\parallel} \sim 5.6l_0$. The strong-coupling case $\omega = 2\Omega_1^0$ with $M = 0.2$ where the analytical prediction (33) does not describe the numerical results due to enhanced intermode coupling [cf Figs. 1 and 2] corresponds to the lowest TE-mode $(1, 1, 1)$ in a cavity of size $l_{\parallel} \sim 22l_0$.

Similarly one can arrange the size of the cavity such

that particular modes are exactly coupled, i.e. Eq. (34) is satisfied. For instance, resonant coupling of the TE-modes $(1, 1, 1)$ and $(4, 1, 1)$ corresponds to $\omega = 2\Omega_1^0$ with $M = \sqrt{7/8}\pi$ [cf Figs. 11 and 12] and is therefore realized in a cavity of size $l_{\parallel} \sim 1.5l_0$. Finally, choosing $l_{\parallel} \sim 0.63l_0$, i.e. $M = \sqrt{5}\pi$, couples the TE-modes $(1, 1, 1)$, $(7, 1, 1)$, $(12, 1, 1)$, $(17, 1, 1)$ and $(22, 1, 1)$ in the resonance case $\omega = 2\Omega_{(1,1,1)}^0$ [cf Figs.13 and 14].

In summary, the mass spectrum Fig. 5 can be interpreted in the following way if we set $n_{\parallel} = 1$ and $\omega = 2\Omega_{(1,1,1)}^0$: For $l_{\parallel} = l_0$, i.e. cubic cavity, the modes $(1, 1, 1)$ and $(5, 1, 1)$ are resonantly coupled (cf. Figs. 9 and 10). Enlarging l_{\parallel} with respect to l_0 increases the production of resonance mode photons $(1, 1, 1)$ until $l_{\parallel} = 1.5l_0$ ($M = \sqrt{7/8}\pi$) is approached where the modes $(1, 1, 1)$ and $(4, 1, 1)$ are exactly coupled (cf. Figs. 11 and 12). When increasing l_{\parallel} further photon creation in the TE-mode $(1, 1, 1)$ becomes more and more efficient and is perfectly described by Eq. (33). Reaching $l_{\parallel} \sim 7.4l_0$ ($M \sim 0.6$, the threshold) the intermode coupling starts to become noticeable causing slight deviations of the numerical results from the analytical prediction. For $l_{\parallel} \sim 11l_0$ ($M \sim 0.4$) the production of TE-mode photons is most efficient. The number of Photons created in the mode $(1, 1, 1)$ is smaller than the analytical prediction Eq. (33) because of the coupling of the modes $(1, 1, 1)$ and $(3, 1, 1)$. When increasing l_{\parallel} beyond $\sim 11l_0$ the strength of the intermode coupling is enhanced drastically and consequently the number of produced TE-mode photons decreases rapidly. For $l_{\parallel} \sim 22l_0$, for instance, the mode $(1, 1, 1)$ is (strongly) coupled to the modes $(3, 1, 1)$ and $(5, 1, 1)$ (cf Fig. 2). Reducing l_{\parallel} with respect to l_0 (i.e. going to masses $M > \sqrt{2}\pi$) lowers the efficiency of photon creation in the resonant mode. The mass spectrum Fig. 15 owns an equivalent interpretation.

VII. CONCLUSIONS

The production of massive scalar particles in a one-dimensional cavity, or analogously the creation of TE-mode photons in a three-dimensional rectangular cavity, has been studied numerically for resonant wall oscillations.

We have found perfect agreement between the numerical results and analytical predictions of [33] in the case that no modes are (strongly) coupled. When two modes are exactly coupled, i.e. Eq. (32) possesses integer solutions for l and k , the numerical results agree with analytical predictions of [33] for sufficiently long times but disagree for short times. The discrepancy for short times is ascribed to properties of the multiple scale analysis used in [33].

The effect of the intermode coupling has been studied in detail which is only possible by means of numerical simulations. As main result we have found that a particular mass exists for which the production of massive scalar

particles is most efficient. The appearance of a maximum in the mass spectrum, i.e. the number of created particles after a given time as function of mass, is explained by the increasing strength of the intermode coupling when decreasing the mass below a certain threshold value.

The analogy between massive scalar particles in a one-dimensional cavity and TE-mode photons in a three-dimensional cavity allows the conclusion that the efficiency of TE-mode photon production from vacuum in a resonantly vibrating rectangular cavity can be controlled (and maximized) by tuning the size of the cavity when keeping the quantum numbers n_y, n_z corresponding to the non-dynamical cavity dimensions fixed.

The main resonance case $\omega = 2\Omega_{(1,1,1)}^0$ has been discussed for a cavity with equally sized non-dynamical dimensions $l_{\parallel} = l_y = l_z$ in detail in section VI. We have shown that photon creation in the resonant mode (1, 1, 1) is most efficient if the size l_{\parallel} of the non-dynamical cavity dimensions is ~ 11 times larger than the dynamical cavity dimension. The existence of a certain cavity size which maximizes photon creation is among other things explained by the fact that intermode coupling takes place even if Eq. (32) is satisfied only approximately. If l_{\parallel} is larger than this value the intermode coupling is so strong that higher frequency modes like (3, 1, 1) and (5, 1, 1) couple to the resonant mode (1, 1, 1) and strongly damp its evolution. Furthermore the coupling of particular field modes by tuning the size of the cavity has been studied. The effects provoked by the intermode coupling can be studied in full detail only by means of numerical methods.

Our findings demonstrate that the intermode coupling in dynamical cavities plays an important role. Even if analytical results are known, numerical simulations are a very useful and indeed necessary tool because only they can completely take into account the intermode coupling. In order to study photon creation associated with the full electromagnetic field in a dynamical cavity also the contribution of the transverse magnetic modes (TM) to the photon production has to be considered. Studying TM-modes numerically represents a more demanding task because of the more complicated so-called generalized Neumann boundary condition these modes are subject to. This will be addressed in a future work.

Acknowledgments

The author is grateful to Ruth Durrer and Cyril Cartier for valuable discussions, carefully reading of the manuscript and useful comments. He would also like to thank Ralf Schützhold and Günter Plunien for discussions and comments on the manuscript. Furthermore the author is much obliged to Diego Dalvit and Emil Mottola for enlightening and interesting discussions as well as their kind hospitality during his visit to the Los Alamos National Laboratory. Finally, the author would like to thank Paulo Maia Neto and Francisco Mazzitelli

for discussions and comments during the Seventh Workshop On Quantum Field Theory Under The Influence Of External Conditions, Barcelona, Spain, 2005. Financial support from the Swiss National Science Foundation is gratefully acknowledged.

APPENDIX A: REMARKS ON NUMERICS

To solve the system of differential equations formed by Eqs. (22) and (23) numerically we decompose $\xi_n^{(m)}(t)$ and $\eta_n^{(m)}(t)$ in their real and imaginary parts:

$$\xi_n^{(m)} = u_n^{(m)} + i v_n^{(m)}, \quad \eta_n^{(m)} = x_n^{(m)} + i y_n^{(m)}. \quad (\text{A1})$$

The resulting coupled system of first-order differential equations can then be written in the form

$$\dot{\underline{X}}^{(m)}(t) = \underline{W}(t)\underline{X}^{(m)}(t) \quad (\text{A2})$$

with real vectors $\underline{X}^{(m)}(t)$ and matrix $\underline{W}(t)$. Choosing the representation

$$\underline{X}^{(m)} = (u_1^{(m)} \dots u_K^{(m)} x_1^{(m)} \dots x_K^{(m)} v_1^{(m)} \dots v_K^{(m)} y_1^{(m)} \dots y_K^{(m)})^T, \quad (\text{A3})$$

where we have truncated the infinite system via introducing the cut-off parameter $K \equiv k_{\max}$, the $4K \times 4K$ - matrix $\underline{W}(t)$ becomes

$$\underline{W}(t) = - \begin{bmatrix} C^-(t) & C^+(t) & -A^+(t) & A^-(t) \\ C^+(t) & C^-(t) & -A^-(t) & A^+(t) \\ A^+(t) & -A^-(t) & C^-(t) & C^+(t) \\ A^-(t) & -A^+(t) & C^+(t) & C^-(t) \end{bmatrix} \quad (\text{A4})$$

with the $K \times K$ - matrices $C^{\pm}(t) = [c_{kn}^{\pm}(t)]$, $1 \leq k, n \leq K$ and diagonal matrices $A^{\pm}(t) = [a_{nn}^{\pm}(t)]$ where $a_{nn}^{\pm}(t)$ and $c_{nk}^{\pm}(t)$ are defined in Eq. (24) and Eq. (25), respectively. The number of particles (18) created in a mode n at $t = t_1$ may now be expressed in terms of the real functions:

$$N_n(t_1) = \frac{1}{4} \sum_{m=1}^K \frac{\Omega_n^1}{\Omega_m^0} \left\{ \left[\Delta_n^-(t_1) u_n^{(m)}(t_1) + \Delta_n^+(t_1) x_n^{(m)}(t_1) \right]^2 + \left[\Delta_n^-(t_1) v_n^{(m)}(t_1) + \Delta_n^+(t_1) y_n^{(m)}(t_1) \right]^2 \right\} \quad (\text{A5})$$

which in the particular case $t_1 = \mathcal{N}T$ with T the period of the cavity oscillations and integer \mathcal{N} reduces to

$$N_n(\mathcal{N}T) = \frac{1}{4} \sum_{m=1}^K \left[\left(x_n^{(m)}(\mathcal{N}T) \right)^2 + \left(y_n^{(m)}(\mathcal{N}T) \right)^2 \right]. \quad (\text{A6})$$

In order to calculate (A5) the system (A2) has to be evolved numerically K -times (m is running from 1 to $K = k_{\max}$) up to $t = t_1$ with initial conditions

$$v_n^{(m)}(0) = x_n^{(m)}(0) = y_n^{(m)}(0) = 0 \quad (\text{A7})$$

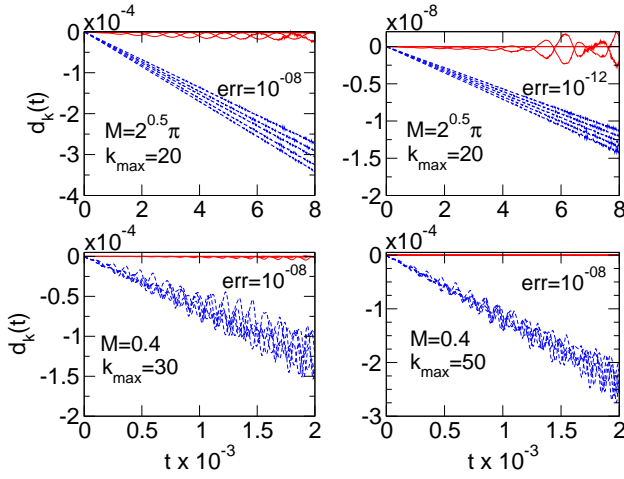


FIG. 18: (color online) The function $d_k(t)$ [Eq. (A11)] for $\omega = 2\Omega_1^0$ and $M = \sqrt{2}\pi$ [panel (a) and (b)] and $M = 0.4$ [panel (c) and (d)]. In any case $d_k(t)$ is shown for $k = 1, \dots, 5$ (upper bands) and the last five values $k = k_{\max} - 4, \dots, k_{\max}$ (lower bands). With “err” we denote the presetted values for the relative and absolute error used in the numerical simulations performed with, in these cases, the Runge-Kutta Prince-Dormand method.

and

$$u_n^{(m)}(0) = 2\delta_{nm}. \quad (\text{A8})$$

Besides investigating the stability of the numerical solutions in dependence on the cut-off K the quality of the numerical solutions can be assessed by checking the validity of the Bogoliubov relations

$$\sum_m [\mathcal{A}_{mn}(t_1)\mathcal{A}_{mk}^*(t_1) - \mathcal{B}_{mn}^*(t_1)\mathcal{B}_{mk}(t_1)] = \delta_{nk} \quad (\text{A9})$$

$$\sum_m [\mathcal{A}_{mn}(t_1)\mathcal{B}_{mk}^*(t_1) - \mathcal{B}_{mn}^*(t_1)\mathcal{A}_{mk}(t_1)] = 0. \quad (\text{A10})$$

In order to solve the system (A2) numerically we applied integration routines based on different standard solvers. Mainly employed were the Runge-Kutta-Fehlberg 4th-5th order method (`rkf45`) and the Runge-Kutta Prince-Dormand method (`rk8pd`). Source codes provided by the

GNU Scientific Library (GSL) [59] as well as the MAT-PACK - Library [60] were used.

In the following we discuss the accuracy of the numerical simulations by considering the quantity

$$d_k(t) = 1 - \sum (|\mathcal{A}_{mk}(t)|^2 - |\mathcal{B}_{mk}(t)|^2), \quad (\text{A11})$$

indicating to what accuracy the diagonal part of the relation (A9) is satisfied by the numerical solutions. Generic examples for $d_k(t)$ are shown in Fig. 18. Panels (a) and (b) correspond to the exact coupling case $M = \sqrt{2}\pi$ (cf. Figs. 9 and 10) with the absolute and relative errors (err) for the Runge-Kutta Prince-Dormand method (`rk8pd`) [59] have been set to 10^{-8} (a) and 10^{-12} (b). Thereby two “bands” are shown. The upper one correspond to $k = 1$ to 5 whereas the lower one correspond to $k = 16$ to $k_{\max} = 20$. The deviation from zero is larger for higher k because these modes are more affected by the truncation of the infinite system through the cut-off k_{\max} . Comparing the absolute value of the maximal deviation of $d_k(t = 8000)$ from zero which is $\sim 3.5 \times 10^{-4}$ for $\text{err}=10^{-8}$ and $\sim 1.5 \times 10^{-8}$ for $\text{err}=10^{-12}$ with the number of particles created in the resonantly excited modes $N_1(t = 8000) \sim 350$ and $N_5(t = 8000) \sim 400$ demonstrates that the numerical simulations guarantee a good accuracy.

In panel (c) and (d) of Fig. 18 we show $d_k(t)$ for the case $M = 0.4$ (cf. Figs. 6 and 7) for the cut-off values $k_{\max} = 30$ (c) and $k_{\max} = 50$ (d). The numerical simulations have been performed with $\text{err}=10^{-8}$ and again two bands are shown corresponding to the first five (upper band) and last five (lower band) values of k . For $k_{\max} = 50$ the deviation of the absolute value of d_k from zero for the last values $k = 46, \dots, 50$ [panel (d)] is slightly larger compared to the deviation for the last five modes for $k_{\max} = 30$. But the deviation of $d_k(t)$ from zero for the first modes $k = 1, \dots, 5$ is smaller for $k_{\max} = 50$ than for $k_{\max} = 30$, i.e. the accuracy for the first modes improves when increasing k_{\max} as it is expected. Comparing $|d_k(t = 2000)| \sim 3 \times 10^{-4}$ for $k_{\max} = 50$ with the number of created particles $N_1(t = 2000) \sim 124$ demonstrates again the accuracy of the numerical simulations. The remaining Bogoliubov relations are satisfied with the same accuracy.

[1] H. B. G. Casimir, Proc. K. Ned. Akad. Wet. **51**, 793 (1948).
[2] G. Plunien, B. Müller, and W. Greiner, Phys. Rept. **134**, 87 (1986).
[3] M. Bordag, U. Mohideen, and V. M. Mostepanenko, Phys. Rept. **353**, 1 (2001).
[4] V. M. Mostepanenko and N. N. Trunov, *The Casimir Effect and its Applications* (Clarendon Press, Oxford, 1997),

[5] K. A. Milton, J.Phys.A: Math. Gen. **37**, R209 (2004).
[6] S. K. Lamoreaux, Phys. Rev. Lett **78**, 5 (1997).
[7] U. Mohideen and A. Roy, Phys. Rev. Lett **81**, 4549 (1998).
[8] A. Roy, C. Y. Lin, and U. Mohideen, Phys. Rev. D **60**, 111101 (1999).
[9] A. Roy and U. Mohideen, Phys. Rev. Lett **82**, 4380 (1999).
[10] G. Bressi, G. Carugno, R. Onofrio, and G. Ruoso, Phys.

- Rev. Lett **88**, 041804 (2002).
- [11] S. K. Lamoreaux, Rep. Prog. Phys. **68**, 201 (2005)
- [12] V. V. Dodonov, in *Nonstationary Casimir effect and analytical solutions for quantum fields in cavities with moving boundaries*, in M. W. Evans (Ed), Modern Nonlinear Optics, Advances in Chemical Physics Series, Wiley, New York, Vol **119**, Part 1, 309 (2001).
- [13] A. Lambrecht, M.-T. Jaekel, and S. Reynaud, Phys. Rev. Lett. **77**, 615 (1996)
- [14] R. Schützhold, G. Plunien and G. Soff, Phys. Rev. A **57**, 2311 (1998).
- [15] V. V. Dodonov and A. B. Klimov, Phys. Rev. A. **53**, 2664 (1996).
- [16] V. V. Dodonov, Phys. Lett. A **213**, 219 (1996).
- [17] V. V. Dodonov, J. Phys. A: Math. Gen. **31**, 9835 (1998).
- [18] J.-Y. Ji, H.-H. Jung, J.-W. Park, and K.-S. Soh, Phys. Rev. A. **56**, 4440 (1997).
- [19] A. B. Klimov and V. Altuzar, Phys. Lett. A **226**, 41 (1997).
- [20] L.-P. Fu, C. K. Duan, and G.-C. Guo, Phys. Lett. A **234**, 163 (1997)
- [21] A. V. Chizhov, G. Schrade and M. S. Zubairy, Phys. Lett. A **230**, 269 (1997)
- [22] C. K. Law, Phys. Rev. Lett. **73**, 1931 (1994).
- [23] C. K. Cole and W. C. Schieve, Phys. Rev. A. **52**, 4405 (1995)
- [24] O. Méplan and C. Gignoux, Phys. Rev. Lett. **76**, 408 (1996)
- [25] D. A. R. Dalvit and F. D. Mazzitelli, Phys. Rev. A. **57**, 2113 (1998).
- [26] P. Wegrzyn, T. Rog, Act. Phys. Pol. **B32**, 129 (2001)
- [27] M. A. Andreatta and V. V. Dodonov, J. Phys. A **33**, 3209 (2000).
- [28] R. de la Llave and N. P. Petrov, Phys. Rev. E **59**, 6637 (1999).
- [29] V. V. Dodonov and A. B. Klimov, and D. E. Nikonov, J. Math. Phys. **34**, 2742 (1993).
- [30] D. A. R. Dalvit and F. D. Mazzitelli, Phys. Rev. A. **59**, 3049 (1999).
- [31] J.-Y. Ji, H.-H. Jung, and K.-S. Soh, Phys. Rev. A. **57**, 4952 (1998).
- [32] D. F. Mundarain and P. A. Maia Neto, Phys. Rev. A **57**, 1379 (1998).
- [33] M. Crocce, D. A. R. Dalvit, and F. D. Mazzitelli, Phys. Rev. A. **64**, 013808 (2001).
- [34] V. V. Dodonov, Phys. Lett. A **207**, 126 (1995).
- [35] A. V. Dodonov, E. V. Dodonov, and V. V. Dodonov, Phys. Lett. A **317**, 378 (2003).
- [36] A. V. Dodonov and V. V. Dodonov, Phys. Lett. A **289**, 291 (2001).
- [37] M. Crocce, D. A. R. Dalvit and F. D. Mazzitelli, Phys. Rev. A. **66**, 033811 (2002).
- [38] V. V. Dodonov, Phys. Lett. A **244**, 517 (1998).
- [39] V. V. Dodonov, Phys. Rev. A **58**, 4147 (1998).
- [40] E. Sassaroli, Y. N. Srivastava, and A. Widom, Phys. Rev. A **50**, 1027 (1994).
- [41] G. Schaller, R. Schützhold, G. Plunien and G. Soff, Phys. Lett. A **297**, 81 (2002).
- [42] G. Schaller, R. Schützhold, G. Plunien and G. Soff, Phys. Rev. A **66**, 023812 (2002).
- [43] G. Plunien, R. Schützhold, and G. Soff, Phys. Rev. Lett. **84**, 1882 (2000)
- [44] R. Schützhold, G. Plunien, and G. Soff, Phys. Rev. A **65**, 043820 (2002).
- [45] H. Jing, Q.-Y. Shi, and J.-S. Wu, Phys. Lett. A **268**, 174 (2000).
- [46] C. K. Law, Phys. Rev. A **51**, 2537 (1995).
- [47] R. Golestanian and M. Kardar, Phys. Rev. Lett. **78**, 3421 (1997).
- [48] C. K. Cole and W. C. Schieve, Phys. Rev. A. **64**, 023813 (2001).
- [49] M. Crocce, D. A. R. Dalvit, F. C. Lombardo, and F. D. Mazzitelli, Phys. Rev. A **70**, 033811 (2004).
- [50] P. A. Maia Neto, J. Phys. A **27**, 2167 (1994)
- [51] P. A. Maia Neto and L. A. S. Machado, Phys. Rev. A **54**, 3420 (1996)
- [52] M. Crocce, D. A. R. Dalvit, F. C. Lombardo and F. D. Mazzitelli, J. Opt. B: Quantum Semiclass. Opt. **7**, S32 (2005).
- [53] M. Ruser, J. Opt. B: Quantum Semiclass. Opt. **7**, S100 (2005).
- [54] M. Ruser, J.Phys.A: Math. Gen. in press, Eprint: quant-ph/0603097
- [55] N. D. Antunes, hep-ph/0310131 v1 (2003).
- [56] L. Li and B. Z. Li, Phys. Lett. A, **300**, 27 (2002).
- [57] A. Fedotov, N. Narozhny, and Y. Lozovik, J. Opt. B: Quantum Semiclass. Opt. **7**, S64 (2005).
- [58] D. A. R. Dalvit, private communication.
- [59] <http://www.gnu.org/software/gsl/>
- [60] <http://www.matpack.de>